Available online at www.sciencedirect.com
SCIENCE DIRECT®
Journal of Solid State Chemistry 177 (2004) 101–108
JOURNAL OF SOLID STATE CHEMISTRY
http://elsevier.com/locate/jssc

$Co_{3-\delta}O_4$ paracrystal: 3D assembly of nanosize defect clusters in spinel lattice

Wen-Hsu Lee and Pouyan Shen*

Institute of Materials Science and Engineering, National Sun Yat-sen University, 80424 Kaohsiung, Taiwan, ROC

Received 3 March 2003; received in revised form 19 May 2003; accepted 30 May 2003

Abstract

Paracrystalline array of defect clusters ca. five times the lattice spacing of the average $Co_{3-\delta}O_4$ spinel structure occurred more or less in a relaxed manner when the sintered $Co_{1-x}O$ polycrystals were air-quenched below the $Co_{1-x}O/Co_{3-\delta}O_4$ transition temperature to activate oxy-precipitation of cube-like $Co_{3-\delta}O_4$ at dislocations. The same paracrystalline spacing was obtained for $Co_{3-\delta}O_4$ when formed via oxidizing/sintering the $Co_{1-x}O$ powders at 800°C in air, suggesting a nearly constant δ value for $Co_{3-\delta}O_4$ in the $T-P_{O_2}$ conditions encountered. The extra cobalt vacancies and Co^{3+} interstitials, as a result of δ value, may form additional 4:1-derived defect clusters for further paracrystalline distribution in the spinel lattice. The nanosize defect clusters self-assembled by columbic interactions and lattice relaxation in ionic crystal may have potential applications as step-wise sensor of oxygen partial pressure at high temperatures.

Keywords: $Co_{3-\delta}O_4$; Spinel; Defect cluster; Paracrystal; TEM

1. Introduction

The paracrystalline distribution is such that the spacing between defects remains fairly constant but the relative lateral translation may occur more variably [1,2]. $Fe_{1-x}O$ having a considerable degree of nonstoichiometry ($x \leqslant 0.15$ [3]) was known to possess defect clusters of 4:1 type with four octahedral vacant sites surrounding one Fe^{3+}-filled tetrahedral interstitial site [4]. When aged at high temperatures, the 4:1 clusters and/or larger units (e.g. 13:4, 16:5 and form a paracrystal [1,2]) order further into Fe_3O_4 spinel or other ordered phases: p'' and p''' [5,6].

Our recent experimental results indicated the $Ni_{1-x}O$ and $Co_{1-x}O$ with a much smaller x (ca. 0.001 [7] and 0.01 [8], respectively) also formed paracrystals when Zr-doped or (Zr,Y) co-doped to increase the defect concentration. For example, Zr-doped or (Zr,Y) co-doped $Ni_{1-x}O$ transforms to a paracrystal and then Ni_3O_4 spinel when annealed at 1300°C or 1600°C [9,10]. In the case of $Co_{1-x}O$, spontaneous oxidation gives place to $Co_{3-\delta}O_4$, a normal type spinel according to magnetic measurements [11]. Such a transformation was known to occur by cooling below 900°C [12]. Paracrystal and the spinel phase, however form above 900°C for (Zr,Y)-codoped $Co_{1-x}O$ [13]. In these two cases, the charge and volume compensating defects due to the introduction of aliovalent dopants are involved in the generation of 4:1 and larger unit of defect clusters. We further proved experimentally in the $Ni_{1-x}O$–CaO system that isovalent but size-mismatched dopant also causes the formation of paracrystal from rock-salt type oxide [14]. It is of interest to find out whether the nonstoichiometric spinel, formed as a $2\times2\times2$ superstructure from rock salt-type oxide, possesses paracrystals as well.

Here we report that paracrystalline distribution of defect clusters with specific interspacing can indeed be induced in $Co_{3-\delta}O_4$ by high temperature oxidation/precipitation of $Co_{1-x}O$ in air. The defect chemistry by which the intrinsic defects were generated in the near-surface and dislocation regions for $Co_{1-x}O$ to nucleate $Co_{3-\delta}O_4$ spinel with paracrystalline distribution of defect clusters is discussed. The present results are interesting because 3D assembly of nanosize defect clusters in ionic crystal is under the influence of columbic interactions and lattice relaxation rather than

*Corresponding author. Fax: +866-7-5254099.
E-mail address: pshen@mail.nsysu.edu.tw (P. Shen).

0022-4596/03/$ - see front matter © 2003 Elsevier Inc. All rights reserved.
doi:10.1016/S0022-4596(03)00324-4

Van der Waals force. With industrial importance, the paracrystal in the hierarchy lattice of $Co_{1-x}O/Co_{3-\delta}O_4$ is expected to affect catalytically active surface/bulk of the cobalt oxides and may have potential applications as step-wise sensor of oxygen partial pressure at high temperatures. Such an understanding is of general interest to research communities of catalysis and solid-state chemistry.

2. Experimental

$Co_{1-x}O$ (Cerac, 2 μm in size) powders were dry pressed at 650 MPa to form pellets ca. 5 mm in diameter and 2 mm in thickness. The pellets were fired at 1600°C for 1 h or 800°C for 100 h in an open-air furnace and quenched in air.

X-ray diffraction (XRD, Cu$K\alpha$, 35 kV, 25 mA, at 0.05° and 2 s per step up to 2θ angle 120°) was used to identify the predominant phases of the fired pellets. The d-spacings were used for least-squares refinement of the lattice parameters. Scanning electron microscopy (SEM, JSM6400 at 20 kV) was used to study the grain size and microstructure of the sintered polycrystals. Thin sections of the fired pellets were Ar-ion milled to electron transparency for analytical electron microscopic (AEM, JEOL 3010) observations at 300 kV. Energy dispersive X-ray (EDX) analysis was performed using K shell counts for Co and O, and the principle of ratio method without absorption correction [15] to confirm that impurities are negligible in the $Co_{1-x}O$ and $Co_{3-\delta}O_4$ phases. Transmission electron microscopy (TEM) was used to characterize paracrystalline distribution of defect clusters within the $Co_{3-\delta}O_4$ spinel and the microstructures of the co-existing $Co_{1-x}O/Co_{3-\delta}O_4$ phases. Selected area electron diffraction (SAED) within a selected area aperture of 1 μm was used to estimate the reciprocal spacing of defect clusters. Lattice imaging coupled with two-dimensional Fourier transform were also used to identify the structures and defects of the $Co_{3-\delta}O_4$ paracrystal.

3. Results

3.1. Spontaneous transformation of $Co_{1-x}O$ upon cooling in air

3.1.1. XRD

XRD indicated the cobalt oxide polycrystals sintered at 1600°C for 1 h in air and air-quenched to room temperature contained a predominant phase of rock salt structure having a room temperature lattice parameter of 0.4263 ± 0.0001 nm (Fig. 1a). This cell parameter is slightly larger than that cooled from 1200°C (0.4260 nm, JCPDS file 9-402) indicating a larger extent of non-stoichiometry x at a high temperature. The minor $Co_{3-\delta}O_4$ spinel and its rather large paracrystalline spacing of defect clusters cannot be resolved by the present XRD technique, but can be characterized by electron diffraction as following.

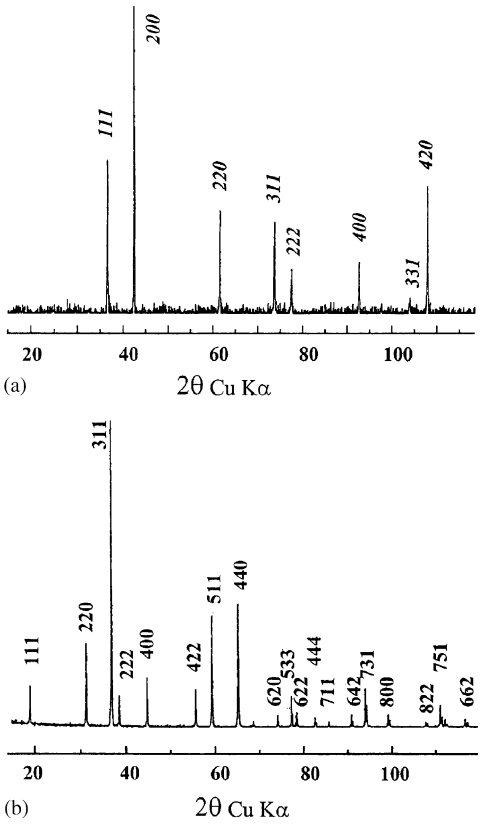

Fig. 1. XRD traces for cobalt oxide polycrystals sintered at (a) 1600°C for 1 h and (b) 800°C for 100 h in air followed by air-quenching to room temperature, showing, respectively, the rock-salt structure peaks of $Co_{1-x}O$ (denoted as italic (hkl)) and the spinel peaks (hkl) of $Co_{3-\delta}O_4$.

3.1.2. Electron microscopy

The sintering process (1600°C for 1 h) of $Co_{1-x}O$ sample caused significant coarsening of the grain size (about 30 μm) as indicated by SEM image (Fig. 2). Cooling below ca. 900°C in air has caused oxidation/precipitation to form cube-like $Co_{3-\delta}O_4$ at dislocations of the host $Co_{1-x}O$ grains (Fig. 3a). Nucleation at dislocations with $\langle 001 \rangle$ line vectors is consistent with our previously observed precipitates of spinel as coherent {001} platelets in Al-doped NiO [16]. The $Co_{3-\delta}O_4$ precipitates are in parallel epitaxy with respect to the host and cause Moiré fringes when the two phases are superimposed (Fig. 3b). The spacing D of the Moiré fringes is given $D = (d_1 d_2)/(d_1 - d_2)$ [17] where d_1 and d_2 are the (200) spacing of $Co_{1-x}O$ (0.2132 nm) and (400) spacing of $Co_{3-\delta}O_4$ (0.2022 nm). The Moiré fringe spacing thus calculated (ca. 3.9 nm) is consistent with that observed in Fig. 3b.

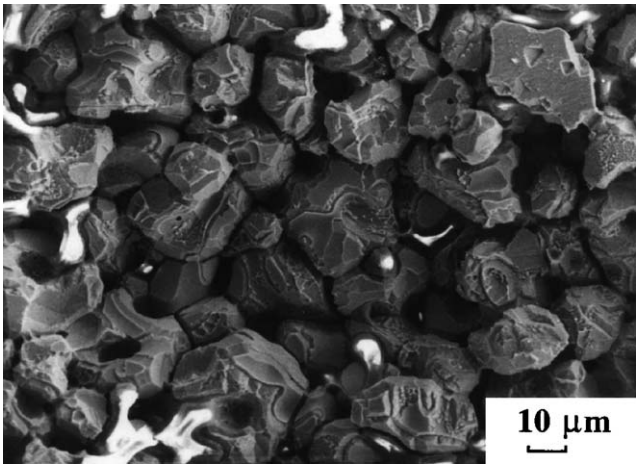

Fig. 2. SEM image of $Co_{1-x}O$ polycrystals sintered at 1600°C for 1 h in air followed by air-quenching and chemical etching (HCl 30 vol% + 2 drops of HF at room temperature for 5 min) to reveal grain boundaries.

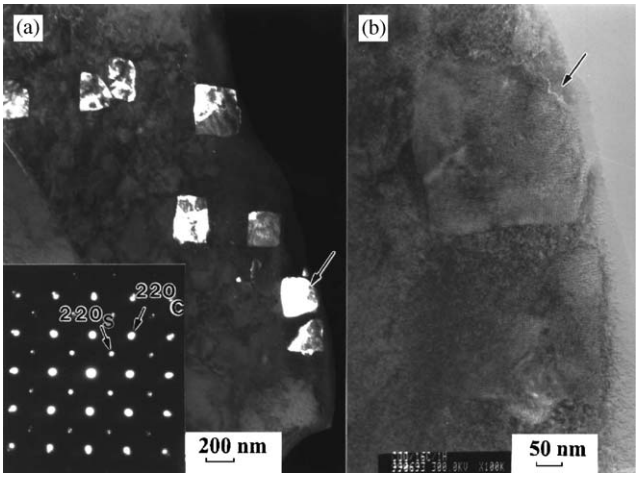

Fig. 3. TEM (a) dark field image of cube-like $Co_{3-\delta}O_4$ spinel (denoted as S) precipitates in a $Co_{1-x}O$ grain (denoted as C) imaged with 220 spinel spot in the inset SAED pattern ($Z = [001]$), and (b) a further magnified view of the arrowed area in (a) (bright field image) showing Moiré fringes for superimposed phases. The same specimen as Fig. 2.

The spinel precipitates were probably nucleated nearly at the same time, such as with specific undercooling below ca. 900°C, in order to be of nearly the same size (Fig. 3) unless coalesced. The lattice image in Fig. 4 shows a rather coherent $Co_{1-x}O/Co_3O_4$ {100} interface full of {110} facets, which indicates that interfacial diffusion and ledge growth may prevail for the oxidation/precipitation process during continuous cooling to room temperature. By contrast, parabolic growth of duplex spinel layers prevailed when (100) $Co_{1-x}O$ was oxidized by cobalt migration outward from Co_3O_4 [18].

The spinel precipitates were commonly found to contain paracrystals giving rise to side band diffraction

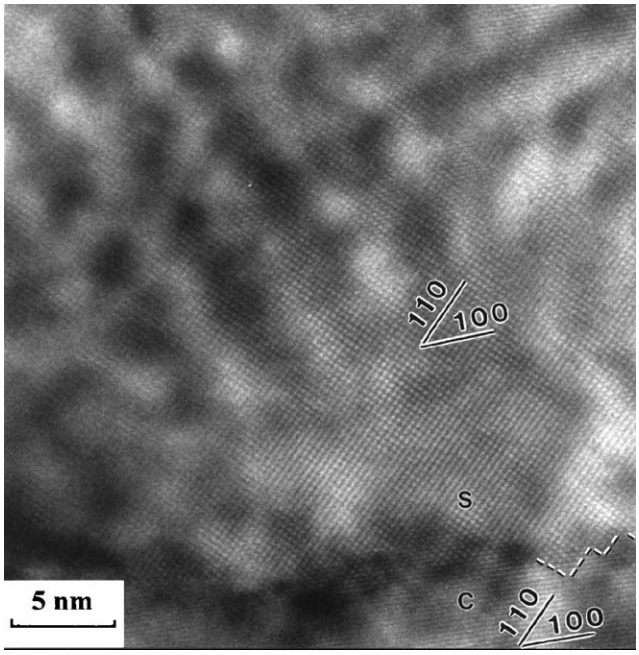

Fig. 4. Lattice image of $Co_{3-\delta}O_4$ spinel precipitated from $Co_{1-x}O$ host with a well-developed and coherent (100) interface decorated with {110} facets (denoted by dashed line). The same specimen as Fig. 2.

spots in the SAED pattern and modulated contrast in the image as represented by those in the zone axes of $[1\bar{1}0]$ and $[1\bar{1}1]$ in Figs. 5a and 6, respectively. The reconstructed image (Fig. 5b) based on the two-dimensional Fourier transform of square region in Fig. 5a indicated that there are dislocations and varied (200) and (111) fringe spacings around dispersed domains with relatively regular spinel lattice (Fig. 5). The paracrystalline spacing (ca. 4.0 nm) is about five times that of the average spinel cell dimension based on side-band spot spacing in the SAED pattern. However, local distribution of defect clusters is less regular according to lattice images taken from local places, such as that shown in Fig. 5b.

3.2. Sintering/transformation of $Co_{1-x}O$ at 800°C in air

3.2.1. XRD

XRD indicated that the cobalt oxide polycrystals sintered at 800°C for 100 h in air contained a predominant phase of $Co_{3-\delta}O_4$ spinel having a room temperature lattice parameter of 0.8086 ± 0.0001 nm (Fig. 1b). This cell parameter is close to that cooled from 850°C (0.8084 nm, JCPDS file 9-418). The $Co_{1-x}O$ relic is too minor in content to be resolved by XRD, but can be clearly identified by electron diffraction as following.

3.2.2. Electron microscopy

The $Co_{1-x}O$ powders sintered at 800°C for 100 h in air were found to oxidize as submicron- to micron-size

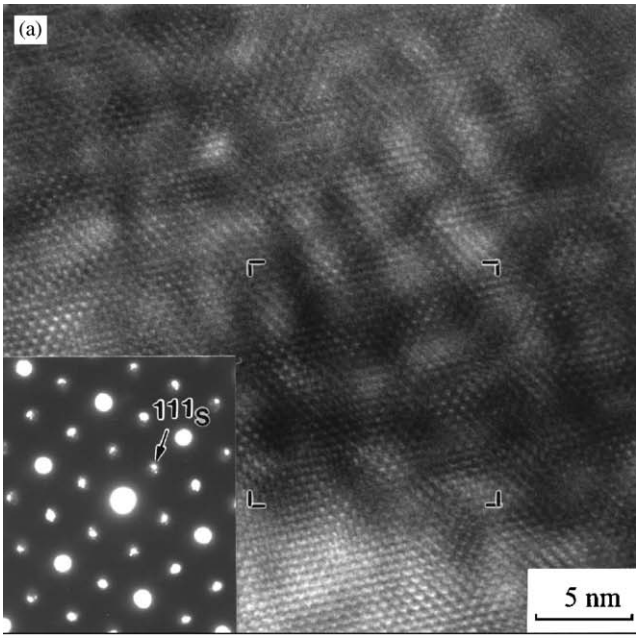

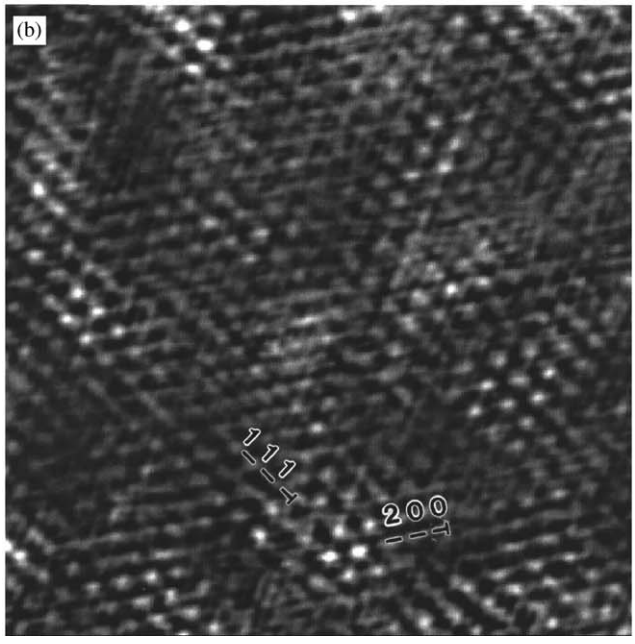

Fig. 5. (a) Lattice image of $Co_{3-\delta}O_4$ showing a paracrystal array. The inset is the corresponding SAED pattern ($Z = [1\bar{1}0]$) showing side-band diffraction spots characteristic of the nanocluster defect paracrystalline distribution. (b) Reconstructed image based on two-dimensional Fourier transform from square region in (a) showing varied (200) and (111) fringe spacing around more regular domains of the spinel lattice with half planes of dislocations delineated by dashed line. The same specimen as Fig. 2.

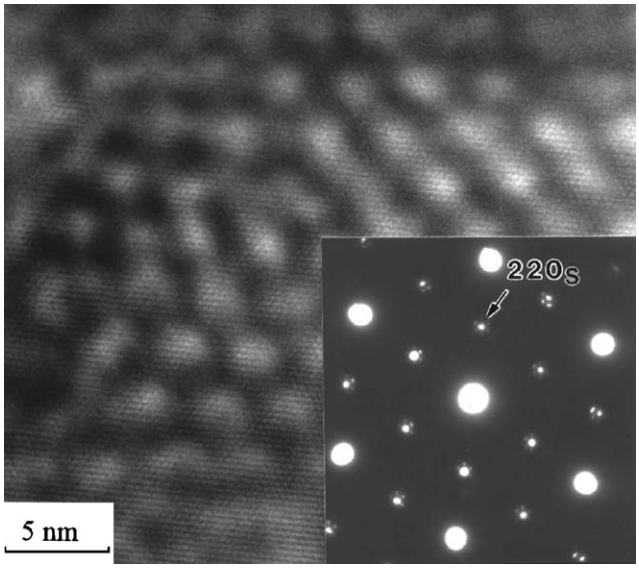

Fig. 6. Lattice image of $Co_{3-\delta}O_4$ showing a paracrystal array. The inset is the corresponding SAED pattern ($Z = [1\bar{1}1]$) showing side-band diffraction spots characteristic of the nanocluster defect paracrystalline distribution. The same specimen as Fig. 2.

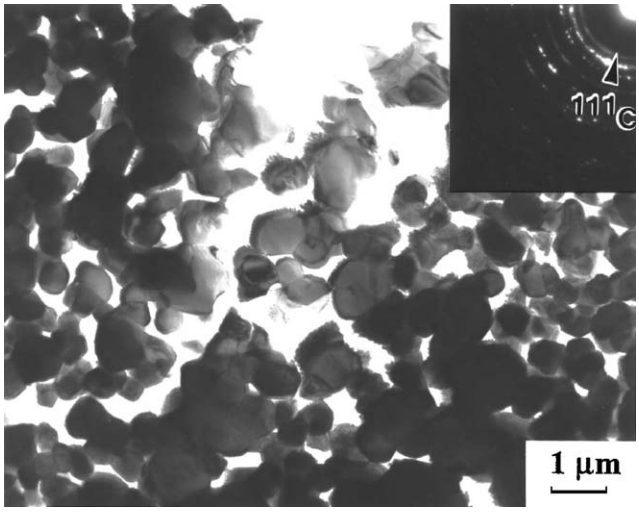

Fig. 7. TEM (bright field image) and inset SAED pattern of $Co_{3-\delta}O_4$/$Co_{1-x}O$ composite polycrystals (with (111) ring of $Co_{1-x}O$ labeled) prepared by sintering $Co_{1-x}O$ powders at 800°C for 100 h in air.

$Co_{3-\delta}O_4$ spinel, as shown by TEM image and inset SAED pattern in Fig. 7. The fired pellets are in fact $Co_{1-x}O/Co_{3-\delta}O_4$ composites with relic nanometersize $Co_{1-x}O$ particles at the frame of the $Co_{3-\delta}O_4$ grains, which have well developed {111} and {100} surfaces as indicated by TEM image and corresponding SAED pattern in Fig. 8. Lattice image in Fig. 9 shows representatively the microstructures in the vicinity of the $Co_{3-\delta}O_4$ (111) surface with attached $Co_{1-x}O$ nanocrystals. These attached particles were predominantly in parallel epitaxy with respect to the spinel upon which they anchored. The two phases shared a coherent interface (111) (Fig. 9) and (100) (not shown), yet still with dislocations to be reconciled and paracrystal to be developed. By contrast, randomly oriented $Co_{1-x}O$ nanoparticles were typically observed far away from $Co_{3-\delta}O_4$ (111) surface as represented by particles labeled as 1, 2 and 3 in Fig. 9. The melting point could be considerably lowered, due to nanophase effect, for the $Co_{1-x}O$ nanoparticles. Under this case, it was able

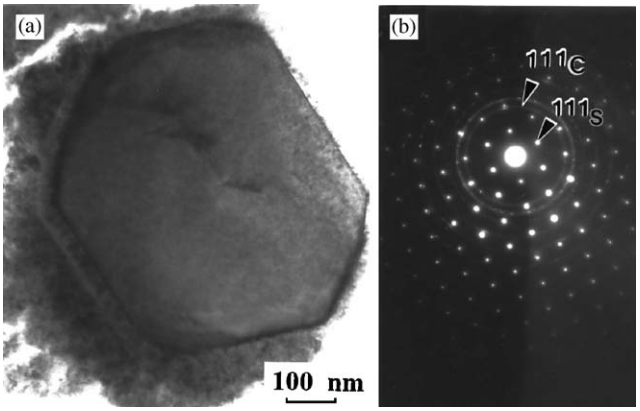

Fig. 8. TEM (a) bright field image and (b) SAED pattern of a cube-octahedral $Co_{3-\delta}O_4$ grain, in $[01\bar{1}]$ zone axis, surrounded by residual nanocrystalline $Co_{1-x}O$ powders in random orientation with (111) diffraction line labeled. The same specimen as Fig. 7.

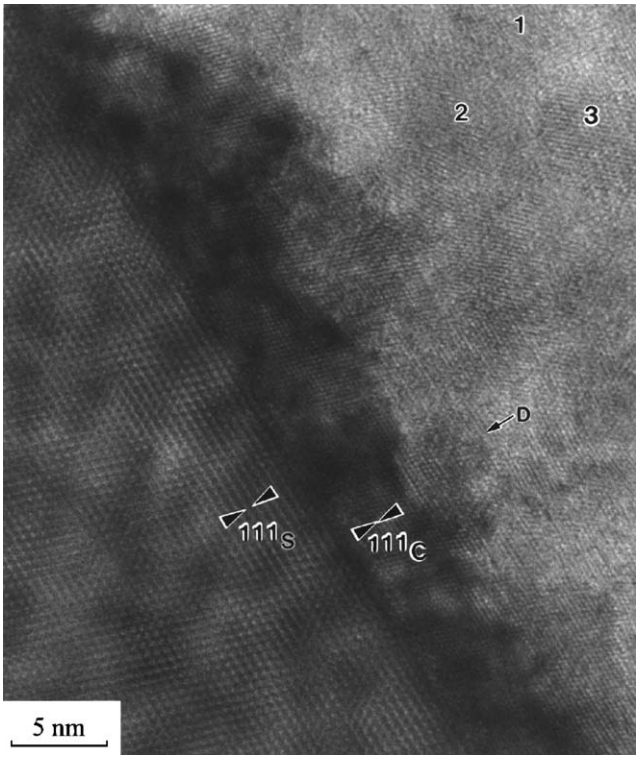

Fig. 9. Lattice image of $Co_{3-\delta}O_4$ (111) surface with attached $Co_{1-x}O$ nanocrystals more or less rotated and coalesced to follow parallel epitaxial relationship with respect to $Co_{3-\delta}O_4$. Note dislocations (designated as D) for imperfectly attached particles and three randomly oriented particles (labeled as 1,2 and 3) far away from $Co_{3-\delta}O_4$ (111) surface. The same specimen as Fig. 7.

to activate Brownian-type rotation of the $Co_{1-x}O$ nanoparticles until they reached epitaxial relationship with respect to the $Co_{3-\delta}O_4$ host. This growth behavior is different from parabolic growth on single crystal surface [18], but is analogous to oxidation-decomposition facilitated reorientation of nanoparticles in reactively sintered $(Ni_{0.33}Co_{0.67})_{1-\delta}O$ polycrystals [19].

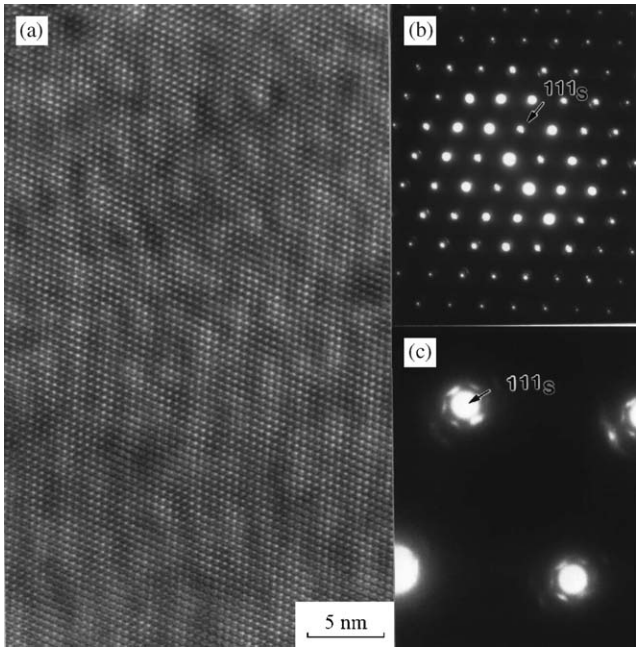

Fig. 10. (a) Lattice image of $Co_{3-\delta}O_4$ single crystal in $[01\bar{1}]$ zone axis showing paracrystalline distribution of defect clusters that give rise to side band spots in SAED pattern (b) and magnified in (c). The same specimen as Fig. 7.

The $Co_{1-x}O$ nanoparticles do not show evidence of paracrystalline distribution of defect clusters, either in the image or SAED pattern. However, the concentration of point defects, as ingredients of paracrystals, may become enriched at the surface of the $Co_{1-x}O$ nanoparticles as discussed later. By contrast, there are paracrystals developing out from much larger spinel grains as represented by the lattice image and corresponding SAED pattern in $[01\bar{1}]$ zone axis (Fig. 10) taken from area without superimposed $Co_{1-x}O$ nanoparticles (Fig. 8). The paracrystalline spacing is nearly the same as that formed by continuous cooling below 900°C. We believe the satellite spots around the Bragg position (Fig. 10c) is of structural origin rather than a result of double diffraction or Moiré fringes. It is true that $Co_{1-x}O$ and $Co_{3-\delta}O_4$ maintain parallel orientation relationship and the calculated spacing of parallel Moiré fringe is about 3.9 nm, comparable to the paracrystal spacing (about 4.0 nm). However, upon tilting away from exact zone axis to circumvent double diffractions and Moiré fringes, the satellite spots of paracrystal still remained. In fact, more than 10 independent observations of much larger $Co_{3-\delta}O_4$ grains (about 1 μm in size) free of superimposed $Co_{1-x}O$ nanoparticles in the sample fired at 800°C confirmed that the paracrystal has nothing to do with Moiré fringes. Besides, the diffuse scattering nature of the satellite diffractions (Fig. 10c) is consistent with an inhomogeneous paracrystal array of defect clusters with additional effect of lattice relaxation around the defect clusters as reported for $Fe_{1-x}O$ [2].

4. Discussion

4.1. Defect chemistry

4.1.1. $T-P_{O_2}$ and near-surface effects

At temperatures below 900°C, $Co_{1-x}O$ oxidizes to $Co_{3-\delta}O_4$ in atmosphere [12]. The generation of electron hole or $Co_{Co}^{3+}\cdot$ in the $Co_{1-x}O$ lattice may proceed through the following equations in Kröger–Vink notation [20]:

$$1/2O_2 \rightarrow V_{Co}^{x} + O_O^{x}, \quad (1)$$

$$V_{Co}^{x} \rightarrow V_{Co}' + h^{\bullet}, \quad (2)$$

$$V_{Co}' \rightarrow V_{Co}'' + h^{\bullet}. \quad (3)$$

V_{Co}' is in fact V_{Co}'' associated with an electron hole localized to form a bound pair of point defects on the octahedral Co sites, i.e. $[V_{Co}''+Co_{Co}^{3+}\cdot]$analogous to the nature of "singly charged nickel vacancies" in $Ni_{1-x}O$ [21]. Below 900°C, Co^{3+} may also reside in the interstitial tetrahedral site to form 4:1 clusters through the following equation [13]

$$Co_{Co}\cdot + 2V_{Co}'' + 2Co_{Co}\cdot \rightarrow [Co_i^{\bullet\bullet\bullet} + 4V_{Co}'' + 4Co_{Co}\cdot], \quad (4)$$

as for dopant-stabilized 4:1 clusters for 3*d* transition metal monoxides, e.g. Fe^{3+}-doped $Ni_{1-x}O$ and Mn^{3+}-doped $Co_{1-x}O$ according to theoretical calculation [22]. Eq. (4) also accounts for the formation of the paracrystals in the $Co_{1-x}O$ phase, which can be further developed into spinel structure having cations ordered in the tetrahedral and octahedral sites [13]. Note in situ work function measurements of the $Co_{1-x}O$ single-crystal cleavage in the temperature range 790–905°C at oxygen partial pressures near the equilibrium with Co_3O_4 indicated that the formation and ionization of cobalt vacancies (Eqs. (1–3)) is much faster than the formation of the $Co_i^{\bullet\bullet\bullet}$donors (Eq. (4)) [23]. In addition, these intrinsic defects preferred to occur at free surface and therefore the Co_3O_4 structure forms within the near-surface layer under $T-P_{O_2}$ conditions, which correspond to the stability of the CoO phase in the bulk [23]. In view of near-surface $Co_{1-x}O/Co_{3-\delta}O_4$ phase diagram [23], the nucleation of $Co_{3-\delta}O_4$ spinel from the sintered $Co_{1-x}O$ polycrystals could possibly start above 900°C upon cooling in atmosphere. Nucleation is expected to occur at the free surface of the sintered pellet as well as at dislocations where intrinsic defects segregate and short-circuit diffusion prevails.

The defect structure of normal $Co_{3-\delta}O_4$, which can be described by the formula $(Co_{tet}^{2+})_8(Co_{oct}^{3+})_{16}(V_{oct})_{16}(O^{-2})_{32}$, is not well known but cation vacancies seem to be predominant lattice defects in this structure [23]. Since $Co_{3-\delta}O_4$ lattice also contains paracrystalline distribution of defect clusters at high temperatures, there might be near-surface consecutive regimes of forming cobalt vacancies and then cobalt interstitials via Eqs. (1)–(4) analogous to the case of parent $Co_{1-x}O$ [23]. The Co^{3+} content exceeding that of stoichiometric Co_3O_4, as denoted by δ in the formula $Co_{3-\delta}O_4$, may occupy both tetrahedral *A* sites and octahedral *B* sites at high temperatures as the case of so-called disordered spinel above 1150 K [24]. On the other hand, the extra cobalt vacancies and Co^{3+} interstitials, as a result of δ value, may form extra 4:1 defect clusters, in the framework of alternating $Co^{2+}O_4$ tetrahedra and $Co_4^{3+}O_4$ cubes which build up into a face centered cubic lattice of 32 oxygen ions [23]. These extra 4:1 defect clusters may more or less link to affect the paracrystal spacing for $Co_{3-\delta}O_4$.

4.1.2. Spacing between defect clusters

The paracrystalline distribution of defect clusters is nearly five times the lattice spacing of the average spinel structure for $Co_{3-\delta}O_4$, i.e. nearly 10 times the lattice spacing of the parent rock salt structure. By contrast, paracrystalline distribution of defect clusters is generally less than 3.5 times the lattice spacing of the average rock salt structure for transition metal monoxides under the influence of extrinsic and intrinsic defects. For examples, the spacing between defect clusters is 2.8 times the lattice parameter of (Zr,Y)-codoped $Co_{1-x}O$ [13], and nearly 3.5 and 2.5 times the lattice parameter of Zr^{4+}-doped $Ni_{1-x}O$ and (Zr,Y)-codoped $Ni_{1-x}O$, respectively [10].

A much smaller paracrystalline spacing for rock salt structure than spinel structure can be rationalized by a higher extent of nonstoichiometry and hence a higher concentration of defect clusters in the former assuming the defect clusters are of the same type in the two hosts and the effect of defect clustering on electronic configuration and interionic distance is negligibly low [25]. If this is indeed the case, then there is about 47 (i.e. $3.6\times3.6\times3.6$) times difference in defect-cluster concentration given the spacing between defect clusters in $Co_{3-\delta}O_4$ is about 3.6 times that of (Zr,Y)-codoped $Co_{1-x}O$ [13]. Given $x=0.01$ for $Co_{1-x}O$ [8], δ can then be roughly estimated to be $\frac{0.01}{47}=0.0002$ for $Co_{3-\delta}O_4$. It is noteworthy that $Co_{1-x}O$ in equilibrium with $Co_{3-\delta}O_4$ may be short of 4:1-derived defect clusters to form paracrystals unless doped with foreign cations to increase the extent of nonstoichiometry.

4.2. Implications of paracrystals in hierarchy lattice

Atom clusters or molecules under the action of Van der Waals interactions could assemble into a 3D array on a crystalline substrate. For example, CdSe (wurtzite-type structure) nanocrystals slightly prolate along the *c*-axis were found to self-organize on quartz substrate as fcc quantum dot superlattice with the *c*-axis of the quantum dots parallel to each other [26]. Accompanied

with XRD and TEM results, the faceting and birefringence determined by optical microscopy under plane polarized light were suggested to be macroscopic evidence for both the ordering of the quantum dots into a 3D array and the net alignment of their unique optical axes within the superlattice. Their arrangement was suggested to maximize the Van der Waals interactions between neighboring dots and with the substrate.

Within an ionic crystal such as $Fe_{1-x}O$ [1,2] and the present $Co_{3-\delta}O_4$, the nanosize defect clusters can also self-assemble in a rather regular manner as paracrystal. In this case, self-organization of defect clusters is made possible via columbic interactions and lattice relaxation around the defect sites rather than Van der Waals interactions. Lattice relaxation around the defect site has been assumed in previous computer simulation of $Fe_{1-x}O$ paracrystal to be in such a way that the average lattice spacing is decreased in the neighborhood of the defects (which scatter less strongly than the rest of the structure) and is relatively increased elsewhere [2]. The present lattice images of $Co_{3-\delta}O_4$ (e.g. Fig. 5) further showed that there are in fact varied (111) and (200) lattice fringe spacing and dislocations associated with defect clusters. The paracrystal with specific spacing in the hierarchy lattice of $Co_{1-x}O/Co_{3-\delta}O_4$ may have potential applications as step-wise sensor of oxygen partial pressure at high temperatures in view of near-surface consecutive regimes of forming cobalt vacancies, cobalt interstitials and then spinel layer over parent $Co_{1-x}O$ [22]. In addition, the paracrystal in the cobalt oxide catalysts is expected to affect catalytically active surfaces, where the spin state of cobalt ions may vary with fluctuations in the strength of the local structure fields. (Optical spectra in UV, visible and near IR wavelength range indicated that the principal peculiarity of the nonstoichiometric films electronic structure compared with "bulk" samples is a stabilization of Co^{3+} ions high-spin configuration in $Co_{3-\delta}O_4$ spinel octahedral sublattice [27].) Furthermore, it is of interest to explore "bulk" properties as a result of specific content of paracrystalline distribution of defect clusters in the hierarchy rock salt-type and spinel structures. The content of paracrystals may be quantitatively determined in future small-angle XRD study.

5. Conclusions

1. $Co_{3-\delta}O_4$ were found to contain paracrystalline array of defect clusters when the sintered $Co_{1-x}O$ polycrystals were air-quenched below the $Co_{1-x}O/Co_{3-\delta}O_4$ transition temperature to activate oxy-precipitation of cube-like $Co_{3-\delta}O_4$ at dislocations or when $Co_{1-x}O$ powders were oxidized upon sintering at 800°C in air.
2. The specific paracrystalline spacing is ca. five times the lattice spacing of the average $Co_{3-\delta}O_4$ spinel structure.
3. The extra cobalt vacancies and Co^{3+} interstitials, as a result of small δ value roughly estimated to be ca. 0.0002 based on paracrystalline spacing, may form additional 4:1-derived defect clusters for $Co_{3-\delta}O_4$ spinel to form paracrystal.
4. The nanosize defect clusters were self-assembled by columbic interactions and more or less relaxed in such a way that dislocations and distorted lattice planes are associated with the defect clusters.
5. The paracrystal in the hierarchy lattice of $Co_{1-x}O/Co_{3-\delta}O_4$ is expected to affect catalytically active surface/bulk of cobalt oxide catalysts and may have potential applications as step-wise sensor of oxygen partial pressure at high temperatures.

Acknowledgments

We thank anonymous referees for constructive comments and Dr. Dershin Gan for reading the manuscript. This research was supported by National Science Council, Taiwan, ROC under contract NSC91-2216-E-110-014 and partly by NanoTechnology Center of NSYSU.

References

[1] T.R. Welberry, A.G. Christy, J. Solid State Chem. 117 (1995) 398–406.
[2] T.R. Welberry, A.G. Christy, Phys. Chem. Miner. 24 (1997) 24–38.
[3] B.E.F. Fender, F.D. Riley, in: L. Eyring, M. O'Keefe (Eds.), The Chemistry of Extended Defects in Non-Metallic Solids, North-Holland, Amsterdam, 1970.
[4] C.R.A. Catlow, B.E.F. Fender, J. Phys. C 8 (1975) 3267–3279.
[5] P. Vallet, P. Raccah, Mem. Sci. Rev. Metall. 62 (1965) 1–29.
[6] B. Andersson, J.O. Sletnes, Acta Crystallogr. Sect. A 33 (1977) 268–276.
[7] H.G. Sockel, H. Schmalzried, Ber. Bunsenges. Phys. Chem. 72 (1968) 745–754.
[8] S.M. Tomlinson, C.R.A. Catlow, J.H. Harding, J. Phys. Chem. Solids 51 (1990) 477–506.
[9] P. Shen, S. Chen, H.S. Liu, Mater. Sci. Eng. A 161 (1993) 135–143.
[10] J. Chen, P. Shen, J. Solid State Chem. 140 (1998) 361–370.
[11] P. Cossee, Rec. Trav. Chim. Pays-Bas 75 (1956) 1089–1096.
[12] M. Oku, Y. Sato, Appl. Surf. Sci. 55 (1992) 37–41.
[13] K.T. Lin, P. Shen, J. Solid State Chem. 145 (1999) 739–750.
[14] M.L. Jeng, P. Shen, Mater. Sci. Eng. A 287 (2000) 1–9.
[15] D.B. Williams, Practical Analytical Electron Microscopy in Materials Science, Philips Electronic Instruments, Inc., Electron Optics Publishing Group, Mahwah, NJ, 1984, p. 157.
[16] S.R. Wang, P. Shen, J. Solid State Chem. 140 (1998) 38–45.
[17] M.H. Loretto, Electron Beam Analysis of Materials, 2nd Edition, Chapman and Hall, London, 1994, p. 169.
[18] K. Przybylski, W.W. Smeltzer, J. Electrochem. Soc. 128 (1981) 897–902.

[19] M.Y. Li, P. Shen, S.L. Hwang, Mater. Sci. Eng. A 343 (2002) 227–234.
[20] F.A. Kröger, H.J. Vink, Solid State Phys. 3 (1956) 307–435.
[21] A. Atkinson, A.E. Hughes, A. Hammou, Philos. Mag. A 43 (1981) 1071–1091.
[22] R.W. Grime, A.B. Anderson, A.H. Heuer, J. Phys. Chem. Solids 48 (1987) 45–50.
[23] J. Nowotny, W. Weppner, M. Sloma, Near-surface defect structure of CoO in the vicinity of the CoO/Co_3O_4 phase boundary, in: J. Nowotny, W. Weppner (Eds.), Non-Stoichiometric Compounds Surfaces, Grain Boundaries and Structural Defects, Kluwer Academic Publishers, Dordrecht, 1989, pp. 265–277.
[24] X. Liu, C.T. Prewitt, Phys. Chem. Mineral. 17 (1990) 168–172.
[25] W.L. Smith, A.D. Hobson, Acta Crystallogr. B 29 (1973) 362–363.
[26] C.B. Murray, C.R. Kagan, M.G. Bawendi, Science 270 (1995) 1335–1338.
[27] I.D. Belov, Yu.E. Roginskaya, R.R. Shifrina, S.G. Gagarin, Yu.V. Plekhanov, Yu.N. Venevtsev, Solid State Commun. 47 (1983) 577–584.